Journal of Solid State Chemistry **150,** 371–376 (2000)
doi:10.1006/jssc.1999.8609, available online at http://www.idealibrary.com on IDEAL®

Ternary Antimonide $EuSn_3Sb_4$ and Related Metallic Zintl Phases

Robert Lam, Jingjun Zhang,[1] and Arthur Mar[2]

Department of Chemistry, University of Alberta, Edmonton, Alberta, Canada T6G 2G2

Received September 8, 1999; in revised form December 2, 1999; accepted December 13, 1999

The ternary Zintl compound europium tin antimonide, $EuSn_3Sb_4$, has been synthesized at 900°C in the presence of a tin flux, and its structure has been determined by single-crystal X-ray diffraction methods. It crystallizes in the orthorhombic space group D_{2h}^{16}-*Pnma* with $a = 9.954(2)$, $b = 4.3516(7)$, $c = 22.650(4)$ Å, and $Z = 4$ at 22°C. $EuSn_3Sb_4$ is isostructural to $SrSn_3Sb_4$; it possesses channels defined by an anionic framework of shared $SnSb_4$ tetrahedra, $SnSb_3$ trigonal pyramids, and Sb–Sb zigzag chains, and it is filled by Eu^{2+} cations. Resistivity measurements indicate weakly metallic behavior for ASn_3Sb_4 (A = Eu, Sr) and the structurally related $Ba_2Sn_3Sb_6$. The anisotropic metallic nature of these compounds is explained through extended Hückel band structure calculations. © 2000 Academic Press

Key Words: **Zintl phase; antimonide; crystal structure; band structure.**

INTRODUCTION

The Zintl concept provides a convenient approach to rationalizing the structure and bonding of many solid-state compounds consisting of an electropositive (alkali metal, alkaline-earth, or rare-earth elements) and an electronegative component (*p*-block elements) (1–4). The diversity of structures that can be explained by this set of rules, which prescribes that the electronegative atoms attain an octet through formation of covalent bonds or presence of lone pairs, is evidence of the ubiquity of this scheme. Since an energy gap is usually expected between occupied (bonding and nonbonding) and unoccupied (antibonding) states in the electronic structure of closed-shell systems, the assumption that Zintl compounds should be semiconductors, in general, may have discouraged the actual measurement of their electronic properties. Especially with the heavier main-group elements, metallic behavior can arise through increased band overlap, diminished band gaps, or partial electron transfer from cations to the anionic network (5). Some of these metallic Zintl phases include La_3In_5 (6) and the CMR materials $A_{14}MnPn_{11}$ (A = Eu, Sr; Pn = Sb, Bi) (7–9).

Previously, we prepared two new ternary alkaline-earth tetrel antimonides, $SrSn_3Sb_4$ (10) and $Ba_2Sn_3Sb_6$ (11), which adopt related structures containing large channels made up of 30-membered rings. We report here the preparation of another member, $EuSn_3Sb_4$, and the resistivity measurements of the entire series. These are metallic Zintl phases whose electronic structures are analyzed through extended Hückel calculations.

EXPERIMENTAL

Synthesis

Single crystals of $EuSn_3Sb_4$ used in the structure determination were obtained from a reaction of a 0.25-g mixture of Eu_2O_3, Nb, and Sb in a 1:2:3 ratio (in an attempt to prepare a pnictide oxide), with an excess of Sn added (Eu_2O_3, 97 mg, 0.28 mmol, 99.99%, donated from Changchun Institute of Applied Chemistry; Nb, 51 mg, 0.55 mmol, 99.8%, Cerac; Sb, 101 mg, 0.83 mmol, 99.995%, Aldrich; Sn, 0.50 g, 4.2 mmol, 99.8%, Cerac). The reactants were loaded into a sealed and evacuated fused-silica tube (8-cm length; 10-mm i.d.), which was heated at 600°C for 5 h and 900°C for 6 days, and then cooled to room temperature over 24 h. Some needle-shaped crystals were obtained after the excess Sn was dissolved with concentrated HCl. Windowless EDX (energy-dispersive X-ray) analysis of these crystals on a Hitachi F2700 scanning electron microscope confirmed the presence of Eu, Sn, and Sb but more significantly showed the absence of Nb and O. (Anal. Calcd. (mol %) for $EuSn_3Sb_4$: Eu, 12; Sn, 38; Sb, 50. Found (average of 10 analyses): Eu, 11(2); Sn, 36(2); Sb, 53(3).) $EuSn_3Sb_4$ can be prepared rationally, albeit in low yield ($\sim$10% as gauged by powder X-ray diffraction), through the direct reaction of the elements at 1000°C for 2 days in an evacuated fused-silica tube. The major competing phases are the binary antimonides SnSb and $EuSb_2$. Arc-melting reactions on pressed pellets of mixtures of the elements result in only these binary antimonides. One member of the solid solution $Sr_{1-x}Eu_x$

[1] On leave from Changchun Institute of Applied Chemistry, Academia Sinica, Changchun 130022, P.R. China.

[2] To whom correspondence should be addressed. Fax: (780) 492-8231. E-mail: arthur.mar@ualberta.ca

0022-4596/00 $35.00

Sn_3Sb_4 ($x = 0.5$) could also be prepared by direct reaction of the elements at 950°C for 2 days, although we have not elaborated the entire series.

Structure Determination

Weissenberg photography revealed Laue symmetry *mmm* and systematic extinctions ($0kl$: $k + l = 2n + 1$; $hk0$: $h = 2n + 1$) consistent with the orthorhombic space groups D_{2h}^{16}-*Pnma* and C_{2v}^{9}-$Pn2_1a$. Final cell parameters were determined from a least-squares analysis of the setting angles of 24 reflections in the range $20° \leq 2\theta(\text{Mo}K\alpha) \leq 38°$ centered on an Enraf–Nonius CAD4 diffractometer. Crystal data and further details of the data collection are given in Table 1.

Calculations were carried out with the use of programs in the SHELXTL (Version 5.0) package (12). Conventional atomic scattering factors and anomalous dispersion corrections were used (13). Intensity data were processed, and face-indexed Gaussian-type absorption corrections were applied. On the basis of similar intensity patterns, the centrosymmetric space group *Pnma* was chosen and the initial atomic positions for $EuSn_3Sb_4$ were taken from those of $SrSn_3Sb_4$ (10). In particular, although Sn and Sb have similar scattering factors, we propose the same ordered model for $EuSn_3Sb_4$ as for $SrSn_3Sb_4$ for reasons discussed previously (10). Refinements were performed using least-squares methods. Since refinements of occupancies lead to values ranging from 98(4) to 102(4)% for all atoms, we accept a fully stoichiometric model. The atomic positions were standardized using STRUCTURE TIDY (14). The final cycle of least-squares refinement on F_o^2 of 50 variables (including anisotropic displacement parameters and an isotropic extinction parameter) and 982 averaged reflections (including those having $F_o^2 < 0$) converged to residuals of $R_w(F_o^2)$ of 0.067 and $R(F)$ (for $F_o^2 > 2\sigma(F_o^2)$) of 0.028. Final values of the positional and isotropic displacement parameters are in Table 2, selected interatomic distances and angles are in Table 3, and further details (CIF, structure amplitudes) are available from A.M.

TABLE 1
Crystallographic Data for $EuSn_3Sb_4$

Formula	$EuSn_3Sb_4$
Formula mass (amu)	995.03
Space group	*Pnma* (No. 62)
a (Å)[a]	9.954(2)
b (Å)[a]	4.3516(7)
c (Å)[a]	22.650(4)
V (Å^3)	981.2(3)
Z	4
ρ_{calc} (g cm^{-3})	6.736
Crystal dimensions (mm)	$0.41 \times 0.03 \times 0.03$
Radiation	Graphite monochromated Mo$K\alpha$, $\lambda = 0.71073$ Å
μ(Mo$K\alpha$) (cm^{-1})	245
Transmission factors	0.274–0.564
2θ limits	$3° \leq 2\theta(\text{Mo}K\alpha) \leq 50°$
Data collected	$-11 \leq h \leq 11$, $-5 \leq k \leq 5$, $0 \leq l \leq 26$
No. of data collected	3382
No. of unique data, including $F_o^2 < 0$	982 ($R_{int} = 0.053$)
No. of unique data, with $F_o^2 < 2\sigma(F_o^2)$	834
No. of variables[b]	50
$R(F)$ for $F_o^2 > 2\sigma(F_o^2)$[c]	0.028
$R_w(F_o^2)$[d]	0.067
Goodness of fit	1.09
$(\Delta\rho)_{max}$, $(\Delta\rho)_{min}$ (e$^-$ Å^{-3})	1.8, −2.2

[a] Obtained from a refinement constrained so that $\alpha = \beta = \gamma = 90°$.
[b] Including an extinction coefficient.
[c] $R(F) = \sum||F_o| - |F_c||/\sum|F_o|$.
[d] $R_w(F_o^2) = [\sum[w(F_o^2 - F_c^2)^2]/\sum wF_o^4]^{1/2}$; $w^{-1} = [\sigma^2(F_o^2) + (0.0367p)^2 + 0.00p]$, where $p = [\max(F_o^2, 0) + 2F_c^2]/3$.

TABLE 2
Positional and Equivalent Isotropic Thermal Parameters for $EuSn_3Sb_4$

Atom	Wyckoff position	x	y	z	U_{eq} (Å^2)[a]
Eu	4c	0.06055(7)	1/4	0.12946(3)	0.0159(2)
Sn(1)	4c	0.27824(10)	1/4	0.24954(4)	0.0192(2)
Sn(2)	4c	0.35009(10)	1/4	0.01098(4)	0.0232(2)
Sn(3)	4c	0.45533(9)	1/4	0.85038(4)	0.0169(2)
Sb(1)	4c	0.03089(9)	1/4	0.76859(3)	0.0171(2)
Sb(2)	4c	0.20417(9)	1/4	0.59370(4)	0.0182(2)
Sb(3)	4c	0.21417(9)	1/4	0.37625(4)	0.0180(2)
Sb(4)	4c	0.57001(9)	1/4	0.52978(4)	0.0194(2)

[a] U_{eq} is defined as one-third of the trace of the orthogonalized U_{ij} tensor.

Resistivity

Two single crystals of each of $EuSn_3Sb_4$, $SrSn_3Sb_4$, and $Ba_2Sn_3Sb_6$ (0.5 to 0.9 mm in length), confirmed by EDX measurements to be the ternary compounds, were mounted with Ag paint on Au wires with graphite extensions. Four-probe ac electrical resistivity measurements were made along the needle axis b of all crystals between 25 and 290 K. The measurements are reproducible between the two samples of each compound.

Band Structure

One-electron band structure calculations on the anionic channel frameworks $[Sn_3Sb_4]^{2-}$ (in $EuSn_3Sb_4$ or $SrSn_3Sb_4$) and $[Sn_3Sb_6]^{4-}$ (in $Ba_2Sn_3Sb_6$) were performed using the EHMACC suite of programs (15, 16). Extended Hückel parameters used for Sn (H_{ii}(eV): −16.16 (5s), −8.32 (5p); ζ_1: 2.12 (5s), 1.82 (5p)) and Sb (H_{ii}(eV): −18.8 (5s), −11.7 (5p); ζ_1: 2.323 (5s), 1.999 (5p)) were taken from literature values

TABLE 3
Selected Interatomic Distances (Å) and Angles (deg) in $EuSn_3Sb_4$

Sn(1)–Sb(1)	2.921(1) (2×)	Eu–Sb(2)	3.2978(9) (2×)
Sn(1)–Sb(3)	2.940(1)	Eu–Sb(1)	3.3007(8) (2×)
Sn(2)–Sb(2)	2.9217(9) (2×)	Eu–Sb(4)	3.3943(8) (2×)
Sn(2)–Sb(4)	2.937(2)	Eu–Sb(3)	3.450(1)
Sn(3)–Sb(2)	2.782(1)	Eu–Sb(4)	3.608(1)
Sn(3)–Sb(1)	2.798(1)	Eu–Sn(1)	3.478(1)
Sn(3)–Sb(3)	2.8150(9) (2×)	Eu–Sn(1)	3.925(1)
Sb(4)–Sb(4)	2.915(1) (2×)	Eu–Sn(2)	3.938(1)
Sb(1)–Sn(1)–Sb(1)	96.31(4)	Sn(3)–Sb(1)–Sn(1)	91.87(3) (2×)
Sb(1)–Sn(1)–Sb(3)	89.82(3) (2×)	Sn(1)–Sb(1)–Sn(1)	96.31(4)
Sb(2)–Sn(2)–Sb(2)	96.27(4)	Sn(3)–Sb(2)–Sn(2)	97.32(3) (2×)
Sb(2)–Sn(2)–Sb(4)	91.49(3) (2×)	Sn(2)–Sb(2)–Sn(2)	96.27(4)
Sb(2)–Sn(3)–Sb(1)	101.49(4)	Sn(3)–Sb(3)–Sn(3)	101.23(4)
Sb(2)–Sn(3)–Sb(3)	116.03(3) (2×)	Sn(3)–Sb(3)–Sn(1)	85.80(3) (2×)
Sb(1)–Sn(3)–Sb(3)	111.20(3) (2×)	Sb(4)–Sb(4)–Sb(4)	96.57(6)
Sb(3)–Sn(3)–Sb(3)	101.23(4)	Sb(4)–Sb(4)–Sn(2)	107.97(4) (2×)

(17, 18). Properties were extracted from the band structure using 80 k points in the irreducible portion of the Brillouin zone (19).

RESULTS AND DISCUSSION

Description of the Structure

In structures of Zintl compounds, the cations play an important role in influencing the shape of the anionic substructure through ionic interactions. Given the values of ionic radii of divalent cations (Eu^{2+}, 1.25; Sr^{2+}, 1.26; Ba^{2+}, 1.42 Å for CN8) (20), it is not surprising that $EuSn_3Sb_4$ and $SrSn_3Sb_4$ are isostructural, while $Ba_2Sn_3Sb_6$ is different. Detailed descriptions of these two structure types, shown down their short b axis in Fig. 1, have been given before (10, 11), but it is instructive to review the major features for the purposes of later discussion of the band structures. Both structures possess channels defined by an anionic framework $^3_\infty[Sn_3Sb_4]^{2-}$, made up of 30-membered rings, and they are constructed from $SnSb_4$ tetrahedra, $SnSb_3$ trigonal pyramids, and Sb–Sb zigzag chains connected in the same sequence but in different conformations. The larger channels in $Ba_2Sn_3Sb_6$ accommodate additional Ba^{2+} cations and isolated Sb–Sb zigzag chains $^1_\infty[Sb_2]^{2-}$ (isosteric with neutral chains of two-bonded chalcogen atoms) to give an overall anionic network $^3_\infty[Sn_3Sb_6]^{4-}$. A comparison of metrical details (Table 4) reveals the relative constancy of the $SnSb_4$ tetrahedra and $SnSb_3$ trigonal pyramids in the three structures, with consistently longer Sn–Sb bonds in the trigonal pyramids reflecting the lower valency of the Sn atoms possessing a lone pair. The Sn–Sb anionic frameworks in $EuSn_3Sb_4$ and $SrSn_3Sb_4$ are practically identical, so any differences in the properties of these two compounds would have to originate with the divalent cation.

Resistivity

Figure 2 shows the electrical resistivities of ASn_3Sb_4 (A = Eu, Sr) and $Ba_2Sn_3Sb_6$ measured along b, the direction along which the channels run. All three compounds are poorly metallic. $EuSn_3Sb_4$ and $SrSn_3Sb_4$ show nearly identical behavior ($\rho_{290} = 3.4 \times 10^{-3}\ \Omega$ cm, $\rho_{25} = 2.2 \times 10^{-3}\ \Omega$ cm, $\rho_{290}/\rho_{25} = 1.5$), and they are both poorer conductors by an order of magnitude than $Ba_2Sn_3Sb_6$ ($\rho_{290} = 3.3 \times 10^{-4}\ \Omega$ cm, $\rho_{25} = 3.9 \times 10^{-5}\ \Omega$ cm, $\rho_{290}/\rho_{25} = 8.5$).

Band Structure

To probe the origin of metallic conductivity and to analyze the bonding more fully in ASn_3Sb_4 (A = Eu, Sr) and $Ba_2Sn_3Sb_6$, the band structures of their anionic frameworks

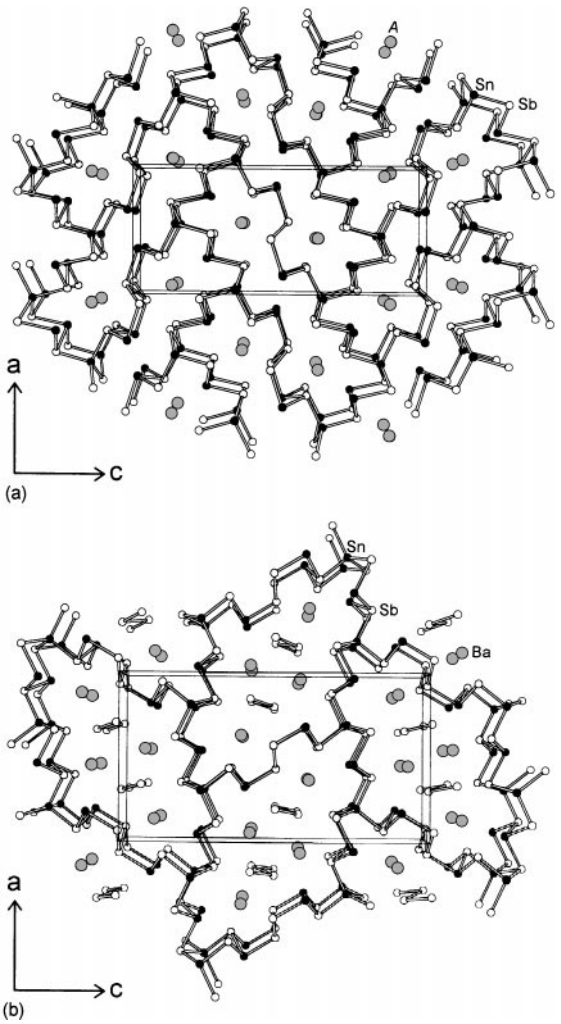

FIG. 1. View down the b axis of the structures of (a) ASn_3Sb_4 (A = Eu, Sr) and (b) $Ba_2Sn_3Sb_6$, with the unit cells outlined. The large lightly shaded circles are Eu, Sr, or Ba atoms, the solid circles are Sn atoms, and the open circles are Sb atoms.

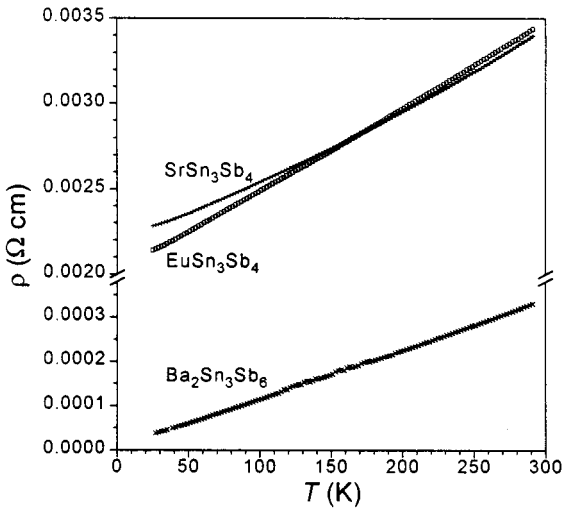

FIG. 2. Plot of resistivity vs temperature for $A\mathrm{Sn_3Sb_4}$ (A = Eu, Sr) and $\mathrm{Ba_2Sn_3Sb_6}$. The resistivity is measured along the needle axis b. Note the axis break.

were calculated. Isolating a single channel from the $^{3}_{\infty}[\mathrm{Sn_3Sb_4}]^{2-}$ framework common to both structure types results in $^{1}_{\infty}[\mathrm{Sn_{14}Sb_{22}}]$, where the coordination of Sb atoms has been completed around all tetrahedral Sn atoms which serve to link neighbouring channels together. As shown in Figs. 3a and 3b, the density of states (DOS) curves for such isolated channels in $A\mathrm{Sn_3Sb_4}$ (A = Eu, Sr) and $\mathrm{Ba_2Sn_3Sb_6}$ are grossly similar, which is expected since they are constructed from the same composition and sequence of building units. Although there are two manifolds of states, the lower energy one originating largely from more electronegative Sb and the higher energy one from less electronegative Sn, there is substantial mixing of Sn and Sb states, indicative of the strong covalent character of the

TABLE 4

Comparison of Distances (Å) and Angles (deg) in $\mathrm{SnSb_4}$ Tetrahedra, $\mathrm{SnSb_3}$ Trigonal Pyramids, and Sb–Sb Zigzag Chains in $A\mathrm{Sn_3Sb_4}$ (A = Eu, Sr) and $\mathrm{Ba_2Sn_3Sb_6}$

	$\mathrm{EuSn_3Sb_4}$	$\mathrm{SrSn_3Sb_4}$	$\mathrm{Ba_2Sn_3Sb_6}$
d(Sn–Sb) tet.	2.782(1)–2.8150(9)	2.788(2)–2.821(1)	2.793(3)–2.840(2)
d(Sn–Sb) trig. pyr.	2.921(1)–2.940(1)	2.920(1)–2.952(2)	2.876(3)–2.913(2)
d(Sb–Sb) zigzag	2.915(1)	2.920(2)	2.902(3)–2.924(2)
<(Sb–Sn–Sb) tet.	101.23(4)–116.03(3)	101.24(6)–115.65(4)	101.89(1)–116.11(7)
<(Sb–Sn–Sb) trig. pyr.	89.82(3)–96.31(4)	90.91(5)–96.64(5)	93.10(7)–98.96(10)
<(Sb–Sb–Sb) zigzag	96.57(6)	96.61(9)	97.9(1)–98.9(1)

bonding within these networks. There is a small band gap (<1 eV) located near −6.5 eV in both cases. If the octets were completed on all atoms making up these isolated channels $^{1}_{\infty}[\mathrm{Sn_{14}Sb_{22}}]$, the charge on this formula unit would be 18−. Such an electron count would indeed just fill up all the lower energy states, leaving a band gap and implying semiconducting behavior. Inclusion of the isolated Sb–Sb zigzag chains within the channels in $\mathrm{Ba_2Sn_3Sb_6}$ introduces additional Sb–Sb bonding and antibonding levels which narrows, but does not completely remove, the energy gap (Fig. 3c).

Of course, these channels do not exist in isolation in the real structures but are linked up to neighboring channels through each of the $\mathrm{SnSb_4}$ tetrahedra. Figure 4a shows how a portion of one channel in the $A\mathrm{Sn_3Sb_4}$ (A = Eu, Sr) structure is connected to a neighboring channel (reference should be made to Fig. 1a to compare with the complete structure). The electron count described above leaves lone pairs on all terminal Sb atoms of the $\mathrm{SnSb_4}$ tetrahedra. Two of these pairs reside in orbitals oriented to form additional Sn–Sb bonds (Fig. 4b), but to avoid repulsive 2c–4e$^-$ interactions, loss of e$^-$ must occur. Effectively, this lowers the

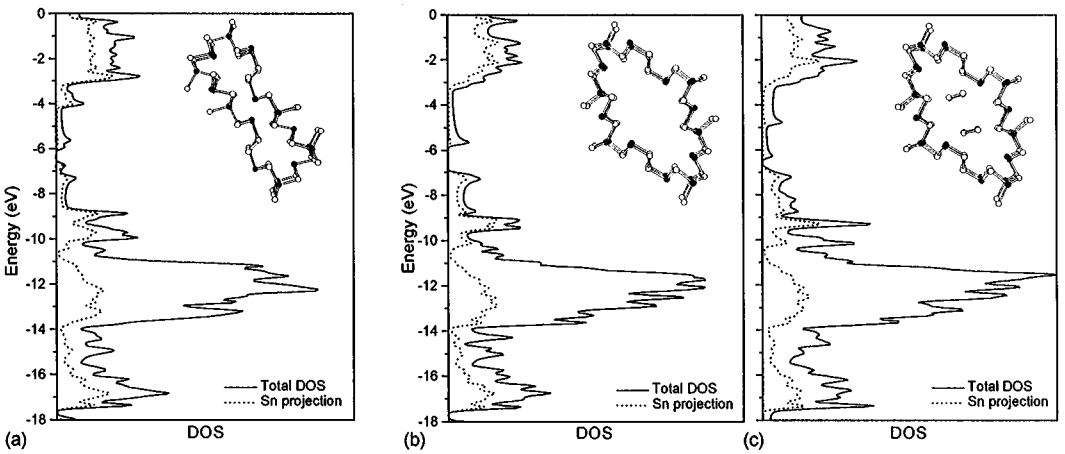

FIG. 3. Density of states (DOS) for isolated one-dimensional channels $^{1}_{\infty}[\mathrm{Sn_{14}Sb_{22}}]$ in (a) $A\mathrm{Sn_3Sb_4}$ (A = Eu, Sr) and (b) $\mathrm{Ba_2Sn_3Sb_6}$ without and (c) with internal $^{1}_{\infty}[\mathrm{Sb_2}]$ zigzag chains included. The Sn projection is shown by the dotted line; what remains of the total DOS is the Sb projection.

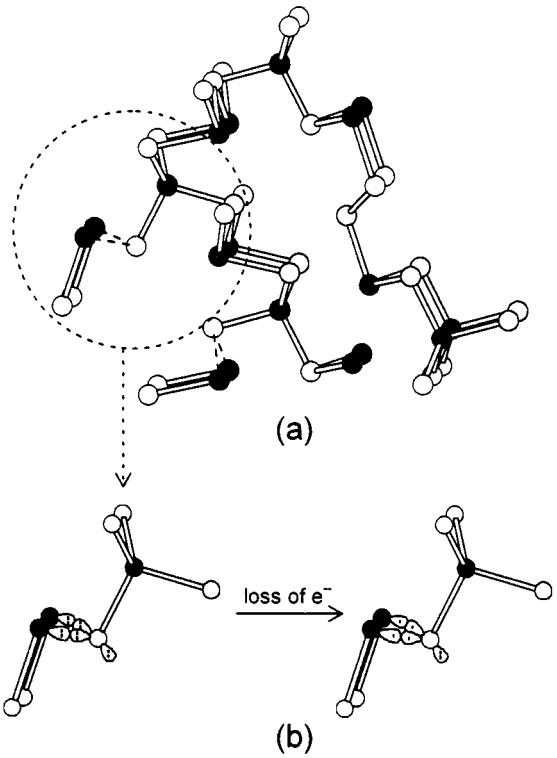

FIG. 4. (a) Portion of the one-dimensional channel in ASn_3Sb_4 (A = Eu, Sr) being connected to a neighboring channel through formation of Sn–Sb bonds (dashed lines). (b) A terminal Sb atom in one of the $SnSb_4$ tetrahedra loses electrons in the formation of Sn-Sb bonds to avoid repulsive interactions.

Fermi level, so that in the DOS curves of the full three-dimensional structures of the anionic frameworks in ASn_3Sb_4 (A = Eu, Sr) and $Ba_2Sn_3Sb_6$ (Fig. 5), the Fermi level lies just below the top edge of the lower energy manifold in a region of low DOS, leading to the observed metallic behavior. Interestingly, the additional interactions arising from linking the channels in the a and c directions are sufficient in themselves to induce further band broadening so that no energy gap is present (Fig. 5).

Figure 6 shows the band dispersion curves along the special directions in the Brillouin zone parallel to the crystallographic axes. In both ASn_3Sb_4 (A = Eu, Sr) and

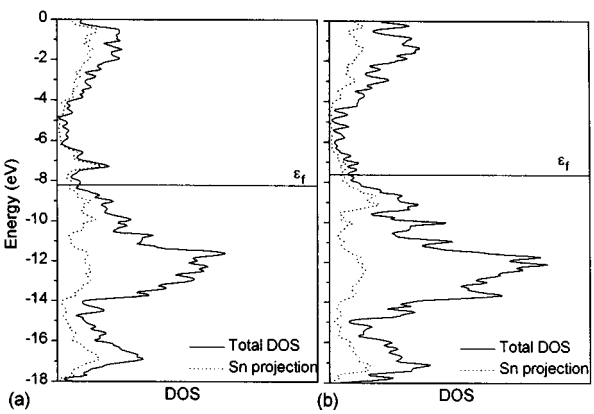

FIG. 5. Total density of states (DOS) for the full three-dimensional anionic substructure of (a) ASn_3Sb_4 (A = Eu, Sr) and (b) $Ba_2Sn_3Sb_6$. The Fermi level (ε_f) is at -8.21 eV for ASn_3Sb_4 and -7.67 eV for $Ba_2Sn_3Sb_6$. The Sn projection is shown by the dotted line; what remains of the total DOS is the Sb projection.

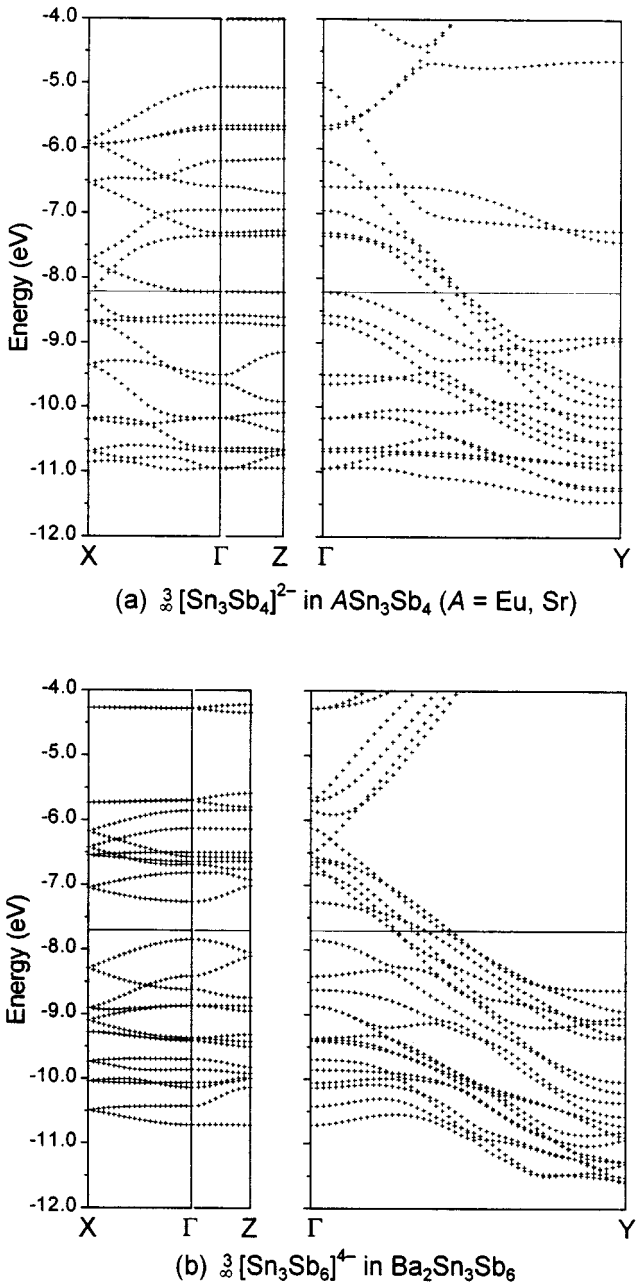

FIG. 6. Band dispersion curves along special symmetry directions for the full three-dimensional anionic substructure of (a) ASn_3Sb_4 (A = Eu, Sr) and (b) $Ba_2Sn_3Sb_6$. The Fermi level is shown by the horizontal line.

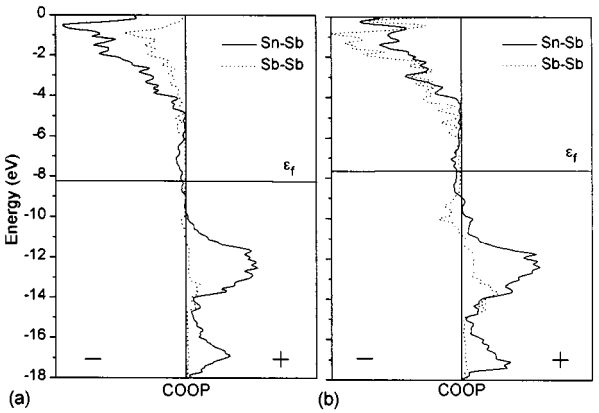

FIG. 7. Crystal orbital overlap population (COOP) curves for ~2.9 Å Sn–Sb (solid line) and Sb–Sb (dashed line) interactions in the full three-dimensional anionic substructure of (a) $A\mathrm{Sn_3Sb_4}$ (A = Eu, Sr) and (b) $\mathrm{Ba_2Sn_3Sb_6}$. The Fermi level is shown by the horizontal line.

$\mathrm{Ba_2Sn_3Sb_6}$, the Fermi level crosses bands of significant dispersion only along ΓY, parallel to the direction along which the channels run. The metallic conductivity is thus predicted to be highly anisotropic, although the small dimensions of the crystals along the other directions have precluded further measurements. The bands crossed by the Fermi level are dispersed over the range −10 to −6 eV in both structure types along ΓY. The better conduction observed in $\mathrm{Ba_2Sn_3Sb_6}$ is probably attributable to the greater number of bands crossed (six) than in $A\mathrm{Sn_3Sb_4}$ (A = Eu, Sr) (four) along ΓY. Analysis of the orbital composition of bands crossed by the Fermi level shows primarily *p* character belonging to atoms comprising the $\mathrm{SnSb_4}$ tetrahedra and $\mathrm{SnSb_3}$ trigonal pyramids (but not the Sb–Sb zigzag chains).

The crystal orbital overlap population (COOP) curves shown in Fig. 7 confirm that predominantly Sn–Sb and Sb–Sb bonding levels are occupied up to the Fermi level. The states from −10 to −6 eV can be associated with contributions from Sn-Sb nonbonding levels, originating from lone pairs on Sn atoms. The cumulated overlap populations are large (Sn–Sb, 0.59; Sb–Sb, 0.55) for these ~2.9 Å interactions, implying full single bonds.

The metallic compounds $A\mathrm{Sn_3Sb_4}$ (A = Eu, Sr) and $\mathrm{Ba_2Sn_3Sb_6}$ may be compared to the series of layered compounds K*Sn*Pn (*Pn* = As, Sb) (21, 22) and $\mathrm{SrSn_2As_2}$ (23), which consist of single or double As-like sheets, respectively, of corner-sharing $\mathrm{Sn}Pn_3$ trigonal pyramids. Calculations suggest that the already small band gap in K*Sn*Pn diminishes even further on going to $\mathrm{SrSn_2As_2}$ because of increased interactions between the sheets (5, 24). In a sense, the walls of the channels in $A\mathrm{Sn_3Sb_4}$ (A = Eu, Sr) and $\mathrm{Ba_2Sn_3Sb_6}$ may be regarded as As-like sheets of $\mathrm{SnSb_3}$ trigonal pyramids that are warped and folded back on themselves. Additional bonding interactions through the formation of $\mathrm{SnSb_4}$ tetrahedra when neighboring channels are adjoined serve as a source of band broadening that leads eventually to the disappearance of the band gap.

ACKNOWLEDGMENTS

This work was supported by the Natural Sciences and Engineering Research Council of Canada and the University of Alberta. We thank Dr. Robert Mcdonald (Faculty Service Officer, X-ray Crystallography Laboratory) for the data collection, and Professor John Beamish (Department of Physics) for access to the resistivity measurement facility.

REFERENCES

1. H. Schäfer, *Ann. Rev. Mater. Sci.* **15,** 1 (1985).
2. J. D. Corbett, *Chem. Rev.* **85,** 383 (1985).
3. H. G. von Schnering, *Angew. Chem. Int. Ed. Engl.* **20,** 33 (1981).
4. S. M. Kauzlarich (Ed.), "Chemistry, Structure, and Bonding of Zintl Phases and Ions." VCH, New York, 1996. [See also references therein].
5. J. K. Burdett, "Chemical Bonding in Solids." Oxford University Press, New York, 1995.
6. J.-T. Zhao and J. D. Corbett, *Inorg. Chem.* **34,** 378 (1995).
7. J. Y. Chan, S. M. Kauzlarich, P. Klavins, R. N. Shelton, and D. J. Webb, *Chem. Mater.* **9,** 3132 (1997).
8. J. Y. Chan, S. M. Kauzlarich, P. Klavins, R. N. Shelton, and D. J. Webb, *Phys. Rev. B: Condens. Matter* **57,** R8103 (1998).
9. D. J. Webb, R. Cohen, P. Klavins, R. N. Shelton, J. Y. Chan, and S. M. Kauzlarich, *J. Appl. Phys.* **83,** 7192 (1998).
10. D. T. Chow, R. McDonald, and A. Mar, *Inorg. Chem.* **36,** 3750 (1997).
11. R. Lam and A. Mar, *Inorg. Chem.* **35,** 6959 (1996).
12. G. M. Sheldrick, "SHELXTL," Version 5.0, Siemens Analytical X-ray Instruments, Inc., Madison, WI, 1994.
13. A. J. C. Wilson (Ed.), "International Tables for X-ray Crystallography," Vol. C. Kluwer, Dordrecht, 1992.
14. L. M. Gelato and E. Parthé, *J. Appl. Crystallogr.* **20,** 139 (1987).
15. M.-H. Whangbo and R. Hoffmann, *J. Am. Chem. Soc.* **100,** 6093 (1978).
16. R. Hoffmann, "Solids and Surfaces: A Chemist's View of Bonding in Extended Structures." VCH, New York, 1988.
17. J. Li and R. Hoffmann, *Z. Naturforsch. B: Anorg. Chem. Org. Chem.* **41,** 1399 (1986).
18. P. Alemany, S. Alvarez, and R. Hoffmann, *Inorg. Chem.* **29,** 3070 (1990).
19. R. Ramírez and M. C. Böhm, *Int. J. Quantum Chem.* **30,** 391 (1986).
20. R. D. Shannon, *Acta Crystallogr. Sect. A* **32,** 751 (1976).
21. K.-H. Lii and R. C. Haushalter, *J. Solid State Chem.* **67,** 374 (1987).
22. J. Klein and B. Eisenmann, *Mater. Res. Bull.* **23,** 587 (1988).
23. B. Eisenmann and J. Klein, *Z. Anorg. Allg. Chem.* **598/599,** 93 (1991).
24. P. C. Schmidt, D. Stahl, B. Eisenmann, R. Kniep, V. Eyert, and J. Kübler, *J. Solid State Chem.* **97,** 93 (1992).